

Growth and Nonlinear Optical Properties of β -Glycine Crystals Grown on Pt Substrates

Ensieh Seyedhosseini,^{*,†} Maxim Ivanov,[†] Vladimir Bystrov,^{†,§} Igor Bdikin,[‡] Pavel Zelenovskiy,^{||} Vladimir Ya. Shur,^{||} Andrei Kudryavtsev,[†] Elena D. Mishina,[†] Alexander S. Sigov,[†] and Andrei L. Kholkin^{†,||}

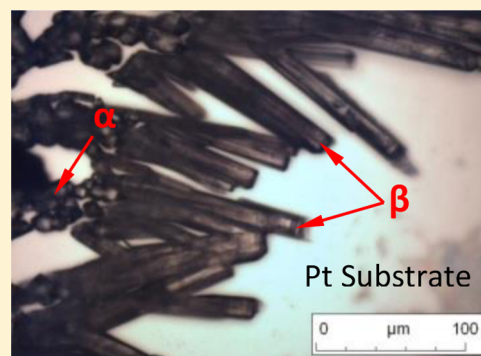
[†]Department of Materials and Ceramic Engineering & CICECO and [‡]Department of Mechanical Engineering & TEMA, University of Aveiro, 3810-193 Aveiro, Portugal

[§]Institute of Mathematical Problems of Biology, 142290 Pushchino, Russia

^{||}Institute of Natural Sciences, Ural Federal University, 620000 Ekaterinburg, Russia

[†]Moscow State Institute of Radioengineering, Electronics, and Automation, 119454 Moscow, Russia

ABSTRACT: Glycine is the simplest amino acid and one of the basic and important elements in biology, as it serves as a building block for proteins. The interest in this material has recently arisen from its useful functional properties, such as its high value of nonlinear optical susceptibility and ferroelectricity. Three polymorphic forms with different physical properties are possible in glycine, the most useful β -polymorph being much less stable than the other two. In this work, we could grow stable microcrystals of β -glycine using a (111)Pt/SiO₂/Si substrate as a template. The effects of the solution concentration and Pt-assisted nucleation on the crystal growth and phase evolution were evaluated using X-ray diffraction analysis and Raman spectroscopy. A second harmonic generation (SHG) method confirmed that the 2-fold symmetry is preserved in as-grown crystals, thus reflecting the expected P2₁ symmetry of the β -phase. Spontaneous polarization direction is found to be parallel to the monoclinic [010] axis and directed along the crystal length. These data are confirmed by computational molecular modeling. Optical measurements revealed also relatively high values of the nonlinear optical susceptibility (50% greater than in the z-cut quartz). The potential use of stable β -glycine crystals in nonlinear optical applications is discussed.



INTRODUCTION

Glycine is the simplest amino acid and is widely used as an excipient for proteins and pharmaceutical reagents production. It has been also recognized as the symbolic origin of life based on its presence in extraterrestrial objects.¹ Glycine as a classical polymorphic material exists in three major polymorphic forms under ambient conditions: α -, β -, and γ -phases. These polymorphs of glycine differ in the packing arrangement of the $^+ \text{NH}_3 - \text{CH}_2 - \text{COO}^-$ zwitterions via a hydrogen-bond network between them. It has been found that the bulk glycine polymorphs display different thermodynamic stability (in the order of $\gamma > \alpha > \beta$) and different crystal symmetry based on different zwitterion packing during growth.² γ - And α -glycine are stable under the ambient conditions, while β -glycine gradually transforms with time into α - or γ -polymorphs. It has been long known that α -glycine crystals are centrosymmetric³ and thus do not exhibit any property described by the third rank tensor such as piezoelectricity or second harmonic generation (SHG). On the contrary, γ ⁴ and β -glycine⁵ polymorphs are strongly noncentrosymmetric and, therefore, can be used as a biocompatible nonlinear optical and piezoelectric material.⁶ Due to its strongly polar nature and

the presence of hydrogen bonds, β -glycine has been long recognized as a potential nonlinear optical (NLO) material in which the useful optical properties (large nonlinear optical coefficient, large birefringence, wide transparency range, high damage threshold, broad spectral and temperature bandwidth, etc.) are combined with the ability of chemical modification using molecular engineering and intrinsic biocompatibility.^{7,8} In addition, recently observed room-temperature ferroelectricity in glycine⁹ opens up new perspectives for using this material in biocompatible nonvolatile memories, optical switches, and transistor gates, to name a few.

In previous works, the β -polymorph of glycine was mostly crystallized by adding antisolvent to a concentrated solution of glycine.^{5,10–12} Other used techniques were spray-drying¹³ and freeze-drying.^{14,15} However, the obtained crystals were frequently unstable under ambient conditions, and rapid conversion into a more stable α -phase was observed in this material.^{5,13} Moreover, some of these methods did not lead to

Received: January 22, 2014

Revised: April 15, 2014

Published: April 18, 2014

the pronounced habit with the well-defined shape, and the grown β -glycine was only present as a mixture with α -crystals. There were a few attempts to stabilize the useful β -phase under ambient conditions. For instance, Hamilton et al.¹⁶ obtained stable nanocrystals of β -glycine embedded in nanometer-scale channels. They found that the nanocrystals grown within the channels of pore diameters less than 24 nm persist for at least 1 year against transformation to other forms and transform slowly to α -glycine over several days if grown within bigger pore diameters. In another paper, Lee et al.^{17,18} studied the effect of the substrate on the polymorph selectivity of glycine. They obtained all three polymorphs of glycine on a patterned substrate with self-assembled monolayers (SAMs) consisting of hydrophilic gold islands surrounded by hydrophobic domains. According to their result, the main crystals phase (in a natural aqueous solution) was an α -phase and the frequency of β -glycine appearance increased for smaller metallic islands and under reducing concentrations. This result was important to understand that the preferential growth of β -glycine can be mediated by using an appropriate substrate that can accelerate the nucleation and further growth of the desired phase.

The goal of this paper was to study the crystallization process of glycine driven by the evaporation of aqueous solution on highly crystalline and chemically active Pt(111) substrates. As a result, we could grow sufficiently stable β -glycine microcrystals with well-defined habit and morphology. This allowed studying their nonlinear optical properties in detail in view of possible applications as active components in nanofibers.¹⁹ We show that the nonlinear optical coefficients of β -glycine are comparable to those of reference *z*-cut (001) quartz. Highly anisotropic second harmonic generation (SHG) signal is found to be compatible with the crystallographic symmetry of β -glycine.

EXPERIMENTAL SECTION

Materials. Glycine powder (99% pure) was purchased from Sigma-Aldrich. Powder X-ray diffraction (PXRD) analysis confirmed that as-received glycine was in the α -form. The droplet evaporation technique was used for the molecular self-assembly and crystal growth on (111)Pt/SiO₂/Si substrates. In this process, the supersaturation and crystallization conditions are controlled by the evaporation rate. Different concentrations of glycine solutions (1.77, 0.66, 0.133, and 0.0133 M) were prepared by dissolving various amounts of glycine powder in an ultrapure water. All solutions were rigorously stirred and filtered before crystallization. Commercial (111)Pt/SiO₂/Si substrates (Inostek) were cleaned with alcohol and pure water in an ultrasonic bath. Glycine solutions were dropped (50 μ L) onto clean surfaces using a micropipet. The surface was left for crystallization under ambient conditions (21 °C, humidity 30%) until the droplet dried out completely.

X-ray Diffraction. XRD patterns of glycine samples were collected with a powder diffractometer (Siemens D500) using Cu K α radiation ($\lambda = 1.540\text{59}\text{\AA}$). The diffraction patterns were recorded in a reflection geometry at room temperature in the range 5°–70° with steps of 0.02°. The single crystal X-ray diffraction data were collected on a Bruker SMART Apex (II) CCD-based diffractometer at 150 K using graphite-monochromatized Mo K α radiation ($\lambda = 0.710\text{73}\text{\AA}$).

Raman Spectroscopy. Micro-Raman measurements were performed in a backscattering geometry using a WiTec alpha 300 AR confocal Raman microscope. An objective (10 \times , NA = 0.55) focused the exciting light (solid state laser, $\lambda = 488\text{ nm}$) onto the sample (spot diameter about 260 nm). A diffraction grating of 600 dashes/mm with a spectral resolution of 3.19 cm⁻¹ at $\lambda = 488\text{ nm}$ was used for light decomposition. All measurements were done at room temperature.

Optical Measurements. The linear optical measurements were used to check the crystal quality and shape of the grown β -glycine

samples. All the measurements were made using an optical microscope (Nikon Eclipse LV 150) with parallel and crossed polarizer and analyzer wave plate modes.

In nonlinear optical measurements (SHG method), the light from a solid-state laser based on a titanium-doped sapphire crystal was used. The output of a Ti:sapphire laser (800 nm) had a pulse width of 100 fs, a repetition rate of 80 MHz, and an average power of 30 mW focused onto a spot of about 50 μ m in diameter. A reflecting geometry was used with the incidence and reflection SHG light fixed at 45° relative to the sample plane. The reflected SHG signal was discriminated by color filters and measured by a photon counting system (see Figure 1 for details).

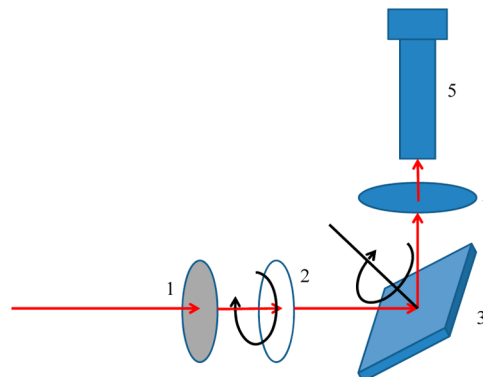


Figure 1. Schematic of the measurement setup for the acquisition of azimuthal and polarization dependences of SHG signal: 1, polarizer; 2, $\lambda/2$ wave plate; 3, sample; 4, analyzer; 5, photomultiplier tube.

For the polarization studies, a polarizer placed in front of the sample and an analyzer placed beyond the sample were used (Figure 1). Thus, the variation in the mutual orientation of the electric field vector for the incident and reflecting beams allowed determination of all components of the nonlinear susceptibility tensors χ which are responsible for the polarization and symmetry dependences. In the following, the electric field vector parallel (perpendicular) to the incidence plane will be termed as P (S) output, respectively.

The relation between the SHG intensity and the electric field of incident light E^{ω} in noncentrosymmetric crystals is proportional to nonlinear polarization squared $I^{\omega} \propto (P_i^{2\omega})^2$ and can be written in a tensor form as

$$P_i^{2\omega} = \chi_{ijk}^{(2)} E_j^{\omega} E_k^{\omega} \quad (1)$$

where $\chi_{ijk}^{(2)}$ is the nonlinear susceptibility tensor defined by the crystallographic structure of the crystal. Analogously to the refractive index (which characterizes the optical properties but also reflects crystallographic structure as well), the nonlinear susceptibility tensor depends on the optical transitions and reflects even more strongly the crystallographic structure. In order to get this information, a set of measurements should be performed, namely, SHG intensity vs azimuthal rotation of the sample and polarization rotation of the incident light.

As a reference sample for the azimuthal and polarization rotation measurements we have used a *z*-cut (001) quartz plate with a well-known nonlinear susceptibility tensor.

RESULTS AND DISCUSSION

Structural Characterization of Microcrystals. Glycine crystals were obtained by the evaporation of microdrops of the water-based solutions on (111)Pt/SiO₂/Si substrates. Powder X-ray diffraction (PXRD) analysis confirmed the existence of all three α -, β -, and γ -polymorphs, but the distribution and the size of grown crystals were strongly dependent on the initial solution concentration. Table I summarizes the presence of

Table 1. Polymorph Distribution of Glycine Crystals Grown on a Pt Surface at 21 °C

conc of glycine	polymorph distribution
133 mg/mL = 1.77 M	α, β, γ
50 mg/mL = 0.66 M	α, β, γ
10 mg/mL = 0.133 M	α, β
1 mg/mL = 0.0133 M	α, β

different glycine polymorphs crystallized on the substrate as a function of the solution concentration. Apparently, all three phases are present in the crystals grown from the concentrated solutions, while only β - and α -phases are observed for lower concentrations. The β -phase being a dominant one will be discussed in detail below.

In order to quantify the phase content, X-ray diffraction patterns were obtained from the crystals attached to the substrate. The spectra were compared with the data available in JCPDS database (00-032-1702 for α -glycine, 00-002-0171 for β -glycine, and 00-006-0230 for γ -glycine). The presence of each phase was revealed by the presence of the corresponding peaks in PXRD data. The positions of peaks substantiate the existence of all glycine phases at higher concentration (1.77 and 0.66 M), while at lower concentrations (0.133 and 0.0133 M) only α - and β -phase were crystallized (Figure 2). Raman spectroscopy was then used for the detailed identification of crystalline forms.

Since we were interested only in β -phase, we focused on the batches grown from the diluted solutions. As an example, Figure 3 demonstrates all three types of crystal morphologies found on the Pt substrate at a 0.133 M concentration: the bipyramidal, the transparent needle-shaped, and the dendrite-type crystals.

We have used the micro-Raman spectroscopy to identify the polymorphic form of each crystal type in the 0.133 and 0.66 M concentration samples. In this technique, a phase analysis was performed by the determination of each phase fingerprints (PF) in Raman spectra and by the comparison of the peak positions with literature data.^{14,18} Raman spectra for three

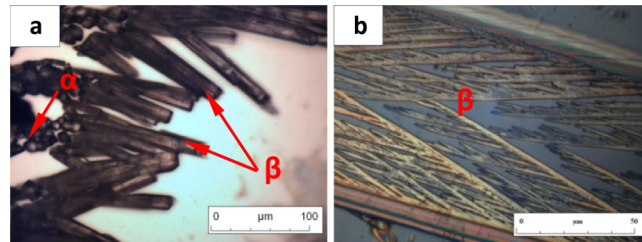


Figure 3. Optical images of (a) bipyramidal α -glycine and needle-shaped β -glycine and (b) dendrite β -glycine.

crystal morphologies are considerably different (Figure 4). In particular, three separate spectral regions, 100–260, 1200–1600, and 2800–3200 cm^{-1} , were compared to distinguish all three polymorphic forms (Figure 3). The first region includes mainly glycine lattice vibrations. Since glycine phases differ in the individual molecule's packing, this region represents the most important PFs. The second spectral region contains bands corresponding to torsional vibrations of the CH_2 group (line at about 1327 cm^{-1}) and symmetrical stretching of the CO_2 group (line at about 1414 cm^{-1}). These lines can be also used as PFs. Probably, the most convenient PF can be found in the third spectral region, where the bands of symmetric and antisymmetric stretching vibrations of the CH_2 group are present. The line position in the vicinity of 2960 cm^{-1} strongly depends on the glycine phase and varies from 2953 cm^{-1} for β -phase up to 2972 cm^{-1} for α -phase. Thus, Raman spectroscopic analysis confirmed that the needle-shaped and dendrite crystals belong to the β -phase, while bipyramidal crystals were all α -phase (Figure 3).

At high solution concentrations, the γ - and β -phases were observed in addition to bipyramidal crystals of α -phase. However, at low solution concentrations, γ -phase is absent, as confirmed by Raman measurements. This observation establishes that the rate of supersaturating generation and drying conditions can control the polymorph selectivity through

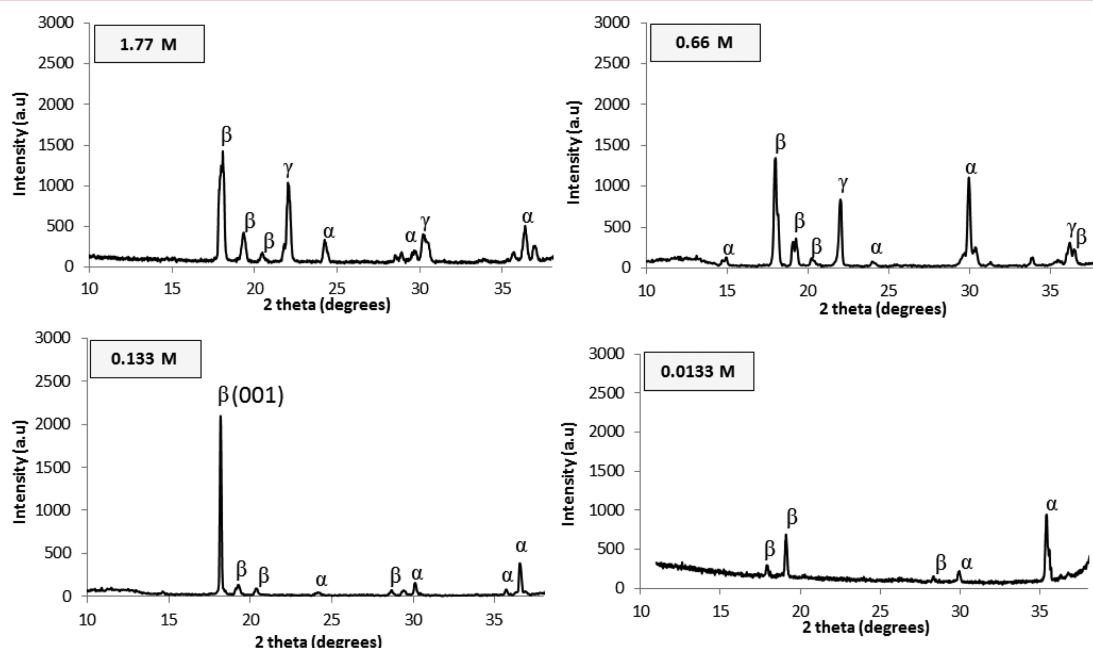


Figure 2. X-ray diffraction patterns of different glycine samples grown on the $\text{Pt}/\text{SiO}_2/\text{Si}$ substrate from the solutions indicated on the figure.

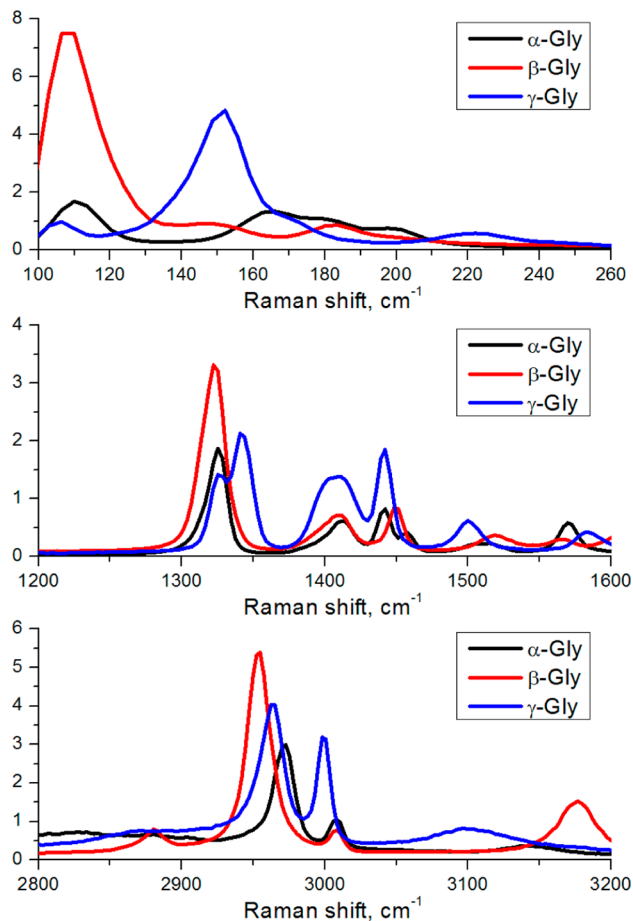


Figure 4. Three spectral regions of the Raman spectra used for the identification of the glycine crystal phases. Measurements were made on samples with 0.133 and 0.66 M concentrations.

changing the crystal growth kinetics and thermodynamics as discussed below.

Crystallization of the needle-shaped β -glycine for all concentrations is in agreement with the basics of Ostwald law²⁰ which states that the crystallization from a solution should start from the nucleation of the least stable polymorph and then it should transform to a more stable phase. It is true also for the glycine-based solutions: we have shown that the less stable β -phase is first formed (Figures 5 and 6). At high concentration (0.66 M) (Figure 5), since the time between the appearance of first β -crystals (Figure 5b) and complete drying (Figure 5e) was sufficiently long (almost 20 min), the β -crystals nucleated at the periphery of the drop could eventually grow to a large size but part of them was readily transformed to α - or γ -phases through the contact with the solution. In the central part of the drop, α -crystals of a bipyramidal shape had also enough time to nucleate and grow.

In contrast, at lower concentrations (0.133 M, Figure 6) β -crystals were the predominant species on the surface, because the solution reached saturation before completely drying, thus nucleation and growth occurred in a few seconds (Figure 6c–e). In other words, β -crystals appear some minutes before drying and do not have time to transform to the undesirable α -phase. As such, nonequilibrium precipitation and fast drying yield the kinetically limited polymorph, β -phase, at the expense of the undesirable γ - and α -phases. After completely drying, β -crystals were stabilized through their contact with the Pt

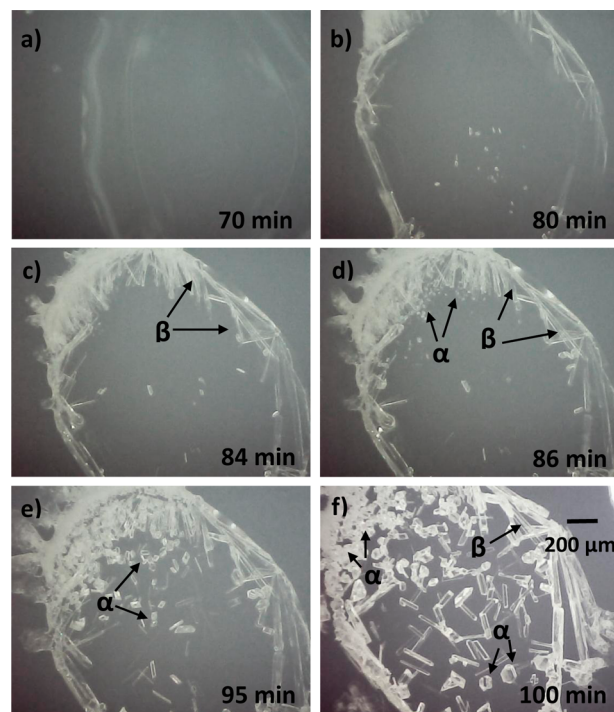


Figure 5. Optical images of the glycine crystals' growth during evaporation of a 0.66 M solution drop on a Pt/SiO₂/Si substrate.

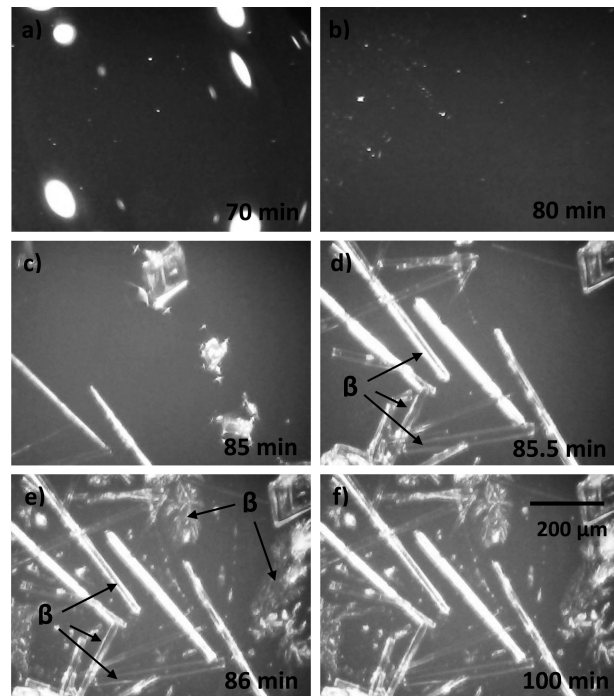


Figure 6. Optical images of the glycine crystals' growth during evaporation of a 0.133 M solution drop on a Pt/SiO₂/Si substrate.

substrate and we did not see any further transformation to an α -phase within 1 month of the shelf time under ambient conditions. The grown β -crystals possessed the same Raman spectra and looked uniform and transparent under a polarized light (Figure 7). The average sizes of β -glycine needle-shaped crystals grown from the diluted solution (about $30 \times 200 \mu\text{m}^2$) were comparable to those reported in the literature.²¹ At 0.133 M concentration, the (001) peak of β -glycine ($2\theta = 18^\circ$) was

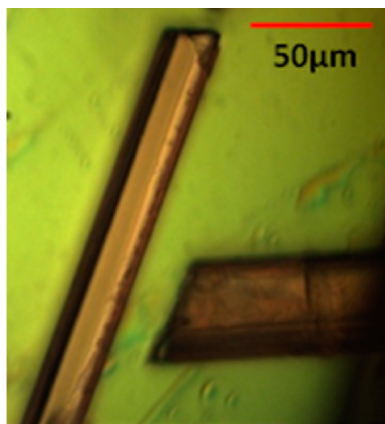


Figure 7. Optical image of β -glycine crystals after 1 month of shelf storage.

considerably increased (Figure 2). This confirms that the (001) crystal planes are parallel to the substrate and that the growth direction of the needle crystals is along the (100) plane (b direction).

In addition, the dendrite β -glycine structure grows very fast on the Pt substrate between microcrystals for low solution concentration. It can be attributed to the interaction between the glycine molecules and the highly crystalline Pt/SiO₂/Si substrate. In general, the nucleation and growth of organic molecular crystals on the crystalline substrates are typically controlled by chemical interactions rather than by the epitaxial relationship.²² The adsorption and surface interaction mechanism of glycine molecule on the Pt surface have been studied a

long time ago.^{23,24} It was reported that the glycine molecules can adsorb on the Pt surface through the oxygen or nitrogen atoms. We believe that, due to this interaction, the Pt surface acts as a nucleation site for glycine crystals through bonding and stabilization of the initial β -phase nuclei. Therefore, it facilitates the growth and prevents further rearrangement of molecules and phase transformation into other phases. Since the solid–solid phase transformation starts from the crystal–substrate interface, chemical interaction of glycine with Pt may prevent this transformation in an adlayer and thus consequently slow down the transformation of the entire crystal. These observations reveal the potential of Pt-coated substrates to control the polymorphic selectivity, stability, and preferred orientation of β -glycine.

In addition to micro-Raman data, the single crystal X-ray diffraction measurements have been done for crystals of needlelike and bipyramidal shapes. The results revealed that the needle-shaped crystals (assigned to β -phase by Raman measurements) belong to the monoclinic system (group $P2_1$) with the following unit cell parameters: $a = 5.08 \text{ \AA}$, $b = 6.25 \text{ \AA}$, $c = 5.36 \text{ \AA}$, $\beta = 113.43^\circ$, $\alpha = \gamma = 90^\circ$. These values are similar to those reported in the literature.⁵ As expected, bipyramidal crystals (α -phase) exhibited reflections characteristic for a monoclinic structure (symmetry $P2_1/n$), and the following cell parameters were extracted: $a = 5.08 \text{ \AA}$, $b = 11.90 \text{ \AA}$, $c = 5.46 \text{ \AA}$, $\beta = 111.29^\circ$, $\alpha = \gamma = 90^\circ$. These values are also in a good agreement with the literature data.²⁵ Therefore, we can conclude that the preferential growth of high-quality glycine β -polymorph was achieved by the careful control of the growth conditions and choice of the suitable substrate.

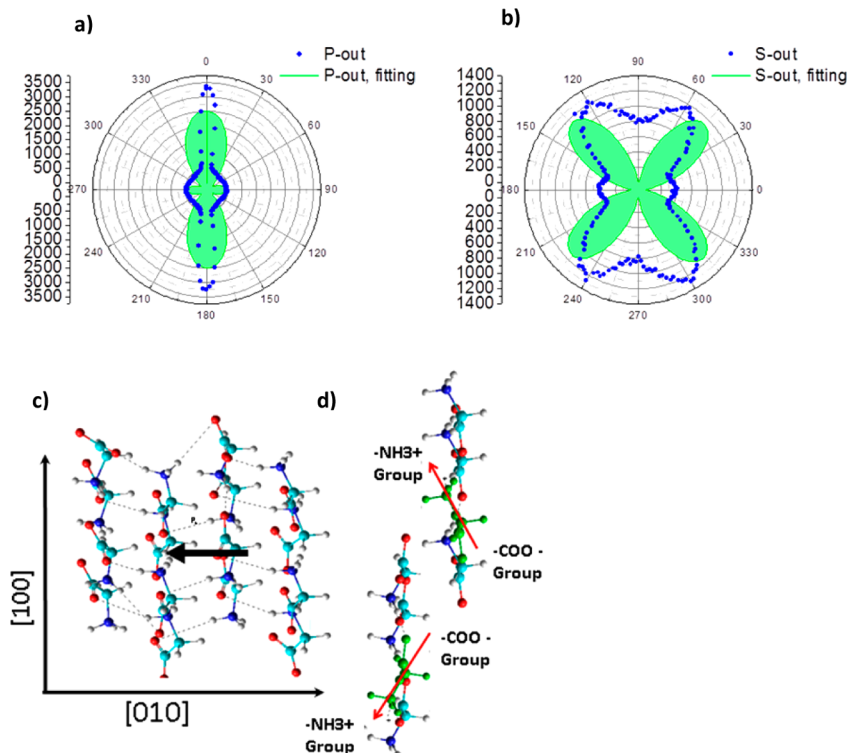


Figure 8. Measured and fitted light polarization dependences of the SHG signal from β -glycine for (a) P and (b) S output polarizations for crystallographic face (001). Molecular simulation of the (c) dipole moment of each glycine molecule as well as molecular cluster cut off from β -glycine crystal consisting of 4 layers and 16 molecules (160 atoms) with corresponding hydrogen bonds and (d) dipole moment of the $-\text{NH}_3^+$, $-\text{COO}^-$ groups of individual (marked by green color) glycine molecule in each layer.

Optical Characterization. During the optical characterization, both linear and nonlinear methods were used. In the linear part, optical images of the grown crystals were acquired with parallel and crossed polarizer and analyzer positions. This procedure allowed finding the crystals where the high-frequency dielectric permittivity looked anisotropic and the highest nonlinear susceptibility of β -glycine polymorph was therefore expected.

Figure 8a,b presents the measured and fitted dependences of the SHG signal oriented parallel (P-out) and perpendicular (S-out) to the polarization of the incident light while rotating this polarization by 360° . In case of [010] crystallographic axes of β -glycine crystal parallel to the incident light polarization direction, two different behaviors for P- and S-output polarization dependences were observed.

For P-output polarization, we have observed two strong 180° peaks (Figure 8a). We assume that these peaks are consistent with the strong dipole contribution of the $-\text{COO}^-$, $-\text{NH}_3^+$ molecule groups aligned along the [010] crystallographic axes (Figure 8c). Therefore, we deduce that the inherent polarization of β -glycine lies along [010] crystallographic axes.

For the S-output polarization, we have observed four strong 180° peaks (Figure 8b). We assume that these peaks contribute to the SHG signal owing to the zwitterions dipole precessions along the [100] crystallographic axes (Figure 8d).

These results are in agreement with the Hyperchem 8²⁶ simulations of the β -glycine molecules in the monoclinic crystal structure. The dipole moment of each molecule as well as the dipole moment of total crystal clusters was calculated using the unrestricted Hartree-Fock (UHF) PM3 method similarly to refs 27–29. The polarization direction is determined from the $-\text{COO}^-$ (carboxylic group) to the $-\text{NH}_3^+$ (amino group) in the zwitterionic form of each individual glycine molecule in polar layers which is nearly normal to the Pt substrate surface (Figure 8c). The layers are linked together in the antiparallel fashion via hydrogen bonds in the [010] direction while forming a monoclinic structure. The total dipole moment is found to be parallel to the native fast-growth crystallographic direction (*b*-axis).

In order to describe the obtained polarization dependences of $I^{2\omega}(\theta)$, eq 1 is rewritten for the point group C_2 and crystal face (001). This gives six independent tensor components: $\chi_1 = \chi_{123} = \chi_{132}$; $\chi_2 = \chi_{113} = \chi_{131} = \chi_{311}$; $\chi_3 = \chi_{322} = \chi_{223} = \chi_{232}$; $\chi_4 = \chi_{333}$; $\chi_5 = \chi_{312} = \chi_{321}$; $\chi_6 = \chi_{213} = \chi_{231}$. The SHG intensity as a function of polarization angle can be expressed as

$$I^{2\omega}(\theta) = C_0 + C_2 \cos 2\theta + C_4 \cos 4\theta + S_2 \sin 2\theta + S_4 \sin 4\theta \quad (2)$$

where C_i and S_i denote the corresponding fitting parameters in the SHG polar dependences, which are the linear combinations of nonlinear susceptibility $\chi_{ijk}^{(2)}$ and Fresnel factors.

The results of the simultaneous fitting of two curves (P- and S-output SHG polarization) are in a good agreement with the nonlinear experimental data (Figure 8a,b, solid lines), showing the amplitude of neighbor molecule oscillation, the same number of petals, and their orientation. These facts confirm our conclusion about the dipole contribution of the $-\text{COO}^-$, $-\text{NH}_3^+$ molecule groups aligned along the [010] crystallographic axes and the zwitterions dipole precessions along the [100] crystallographic axes. This gives the following values of nonlinear susceptibility tensor components: $\chi_1 = 0.36 \text{ pm/V}$, $\chi_2 = 0.73 \text{ pm/V}$, $\chi_3 = 0.16 \text{ pm/V}$, $\chi_4 = 0.28 \text{ pm/V}$, $\chi_5 = 0.89 \text{ pm/V}$,

$\chi_6 = 7.5 \times 10^{-4} \text{ pm/V}$. The absolute values were obtained using a *z*-cut (001) quartz with its nonlinear susceptibility tensor components equal to $\chi_1 = 0.8 \text{ pm/V}$, $\chi_2 = 0.017 \text{ pm/V}$.³⁰ However, the experimental dependences possessed a noticeable background at their minimum (theoretical curves should vanish to zero at the same points). Such deviation may arise due to several reasons, for example, it can be a result of the presence of 90° domains^{31,32} or originate from the light scattering on optical inhomogeneities.

CONCLUSIONS

In summary, we found in this work that the interplay between the concentration of the glycine solution and crystallization effect of the surface, results in the preferential growth of glycine β -phase with well-defined shape and morphology. These two parameters are supposed to be the major factors dictating the evaporation rate and growth kinetics. As a result, β -glycine needle-shaped crystals with the average size of $30 \times 200 \mu\text{m}^2$ could be grown under ambient conditions. No encapsulation in polymers or nanopores was required to maintain the stability of β -phase. X-ray diffraction analysis and Raman spectroscopy confirmed the preferential growth and stability of β -phase. The conducted nonlinear optical measurements were consistent with the P_{21} symmetry of β -glycine with spontaneous polarization parallel to the monoclinic *b*-axis and zwitterions dipole precessions along the *a*-axis. The nonlinear optical susceptibility of β -glycine is found to about 50% greater than that of well-known nonlinear material *z*-cut (001) quartz. Thus, these crystals can be used to transform infrared and visible light into UV and near-UV radiation. Not only frequency conversion, but also amplitude and phase modulation can be used for optical communications and interconnections, optical switching data storage, and electro-optic applications.^{33–35} The intrinsic biocompatibility expected in glycine could be helpful for bioimaging and photothermal therapy,^{36,37} where a light conversion to the UV is required for the generation of short-lived toxic oxygen radicals. Further work is needed to explore the potential of glycine for these applications.

AUTHOR INFORMATION

Corresponding Author

*Phone: +351 234 372 571. Fax: +351 234 401 470. E-mail: seyedhosseini@ua.pt

Notes

The authors declare no competing financial interest.

ACKNOWLEDGMENTS

The work is supported by the European Commission within FP7 Marie Curie Initial Training Network “Nanomotion” (grant agreement no. 290158), by the Russian Ministry of Education and Science (grant no. 14.B37.21.1208), by the Government of Sverdlovsk region (grant no. 13-02-96041-r-Ural-a), and by RFBR (grant no. 13-02-01391-a). The work in CICECO is partly supported by the FCT grant Pest-C/CTM/LA0011/2013 and SFRH/BPD/22230/2005. The equipment of the Ural Center for Shared Use “Modern Nanotechnology” of Institute of Natural Sciences, Ural Federal University has been used. The author thanks Dr. D. Isakov for the help with measurements and enlightening discussions.

■ REFERENCES

- (1) Elsila, J. E.; Dworkin, J. P.; Bernstein, M. P.; Sandford, S. A. *Astrophys. J.* **2007**, *660*, 911–918.
- (2) Pervolich, G. L.; Hansen, L. K.; Bauer-Brandl, A. *J. Therm. Anal. Calorim.* **2001**, *66*, 699–715.
- (3) Albrecht, G.; Corey, R. B. *J. Am. Chem. Soc.* **1939**, *61*, 1087–1103.
- (4) Itaya, Y. *Acta Crystallogr.* **1961**, *14*, 1–10.
- (5) Itaya, Y. *Acta Crystallogr.* **1960**, *13*, 35–45.
- (6) Irimia-Vladu, M.; Troshin, P. A.; Reisinger, M.; Shmygleva, L.; Kanbur, Y.; Schwabegger, G.; Bodea, M.; Schwödiauer, R.; Mumyatov, A.; Fergus, J. W.; Razumov, V. F.; Sitter, H.; Sariciftci, N. S.; Bauer, S. *Adv. Funct. Mater.* **2010**, *20*, 4069–4076.
- (7) Hofmann, G.; Neumann, N.; Budzier, H. *Ferroelectrics* **1992**, *133*, 41–45.
- (8) Pepinsky, R.; Vedam, K.; Hoshino, S.; Okaya, Y. *Phys. Rev.* **1958**, *111*, 430–432.
- (9) Heredia, A.; Meunier, V.; Bdikin, I. K.; Gracio, J.; balke, N.; Jesse, S.; Tselev, A.; Agarwal, P. K.; Sumpter, B. G.; Kalinin, S. V.; Kholkin, A. L. *Adv. Funct. Mater.* **2012**, *22*, 2996–3003.
- (10) Ksanda, C. J.; Tunell, G. *Am. J. Sci.* **1938**, *A 35*, 173–178.
- (11) Drebushchak, V. A.; Boldyreva, E. V.; Drebushchak, T. N.; Shutova, E. S. *J. Cryst. Growth* **2002**, *241*, 266–268.
- (12) Boldyreva, E. V.; Drebushchak, V. A.; Drebushchak, T. N.; Paukov, I. E.; Kovalevskaya, Y. A.; Shutova, E. S. *J. Therm. Anal. Calorim.* **2003**, *73*, 409–418.
- (13) Sander, A.; Penović, T.; Šipušić, J. *Cryst. Res. Technol.* **2011**, *46*, 145–152.
- (14) Surovtsev, N. V.; Adichtchev, S. V.; Malinovsky, V. K.; Ogienko, A. G.; Drebushchak, V. A.; Manakov, A. Yu.; Anchakov, A. I.; Yunoshev, A. S.; Boldyreva, E. V. *J. Chem. Phys.* **2012**, *137*, 065103–1–065103–10.
- (15) Pyne, A.; Suryanarayanan, R. *Pharm. Res.* **2001**, *18*, 1448–1454.
- (16) Hamilton, B. D.; Hillmyer, M. A.; Ward, M. D. *Cryst. Growth Des.* **2008**, *8*, 3368–3375.
- (17) Lee, A. Y.; Lee, I. S.; Myerson, A. S. *Chem. Eng. Technol.* **2006**, *29*, 281–285.
- (18) Lee, I. S.; Kim, K. T.; Lee, A. Y.; Myerson, A. S. *Cryst. Growth Des.* **2008**, *8*, 108–113.
- (19) Isakov, D.; de Matos Gomes, E.; Bdikin, I.; Almeida, B.; Belsley, M.; Costa, M.; Rodrigues, V.; Heredia, A. *Cryst. Growth Des.* **2011**, *11*, 4288–4291.
- (20) Van Santen, R. A. *J. Phys. Chem.* **1984**, *88*, 5768–5769.
- (21) Ferrari, E. S.; Davey, R. J.; Cross, W. I.; Gillon, A. L.; Towler, C. S. *Cryst. Growth Des.* **2003**, *3*, 53–60.
- (22) Olmsted, B. K.; Ward, M. D. *CrystEngComm* **2011**, *13*, 1070–1073.
- (23) Ernst, K. H.; Christmann, K. *Surf. Sci.* **1989**, *224*, 277–310.
- (24) Huerta, F.; Morallon, E.; Cases, F.; Rodes, A.; Vazquez, J. L.; Aldaz, A. J. *Electroanal. Chem.* **1997**, *421*, 179–185.
- (25) Marsh, R. E. *Acta Crystallogr.* **1958**, *11*, 654–663.
- (26) HyperChem (2002), *Tools for Molecular Modeling (release 7, 8)*. Professional edition; Hypercube Inc., Gainesville, FL; <http://www.hyper.com/?tabid=360>.
- (27) Bdikin, I.; Bystrov, V.; Delgadillo, I.; Gracio, J.; Kopyl, S.; Wojtas, M.; Mishina, E.; Sigov, A.; Kholkin, A. L. *J. Appl. Phys.* **2012**, *111*, 074104.
- (28) Bystrov, V. S.; Paramonova, E. V.; Bdikin, I. K.; Bystrova, A. V.; Pullar, R. C.; Kholkin, A. L. *J. Mol. Model.* **2013**, *19*, 3591–3602.
- (29) Bystrov, V. S. *Physica B* **2014**, *432*, 21–25.
- (30) Boyd, R. W. *Nonlinear Optics*; Academic Press: San Diego, CA, 2003.
- (31) Gopalan, V.; Raj, R. *Appl. Phys. Lett.* **1996**, *68* (no.10), 1323–1325.
- (32) Mishina, E. D.; Sherstyuk, N. E.; Barskiy, D. R.; Sigov, A. S.; Golovko, Yu. I.; Mukhorotov, V. M.; Santo, M. De.; Rasing, Th. *J. Appl. Phys.* **2003**, *93*, 6216–6222.
- (33) Salem, R.; Foster, M. A.; Turner, A. C.; Geraghty, G. F.; Lipson, M.; Gaeta, A. L. *Nat. Photonics* **2008**, *2*, 35–38.
- (34) Liao, L.; Liu, A.; Rubin, D.; Basak, J.; Chetrit, Y.; Nguyen, H.; Cohen, R.; Izhaky, N.; Paniccia, M. *Electron. Lett.* **2007**, *43*, 1196–1197.
- (35) Rong, H.; Liu, A.; Jones, R.; Cohen, O.; Hak, D.; Nicolaescu, R.; Fang, A.; Paniccia, M. *Nature* **2005**, *433*, 292–294.
- (36) Hung, H.-S.; Tang, C.-M.; Lin, C.-H.; Lin, S.-Z.; Chu, M.-Y.; Sun, W.-S.; Kao, W.-C.; Hsieh, H.-H.; Huang, C.-Y.; Hsu, S.-h. *PLoS One* **2013**, *8*, e65738.
- (37) Han, J.; Li, J.; Jia, W.; Yao, L.; Li, X.; Jiang, L.; Tian, Y. *Int. J. Nanomedicine* **2014**, *9*, 517–526.